Nano Energy 97 (2022) 107180

Contents lists available at ScienceDirect

Nano Energy

journal homepage: www.elsevier.com/locate/nanoen

Biomass-derived nanostructured coatings based on cellulose nanofibers-melanin hybrids toward solar-enabled multifunctional energy management

Weiqing Yang [a,b,1], Peng Xiao [a,b,1,*], Feng Ni [a,b], Chang Zhang [a,b], Jincui Gu [a,b], Shiao-Wei Kuo [c], Qingquan Liu [d], Tao Chen [a,b,*]

[a] Key Laboratory of Marine Materials and Related Technologies, Zhejiang Key Laboratory of Marine Materials and Protective Technologies, Ningbo Institute of Materials Technology and Engineering, Chinese Academy of Sciences, Zhongguan West Road 1219, Ningbo 315201, China
[b] School of Chemical Sciences, University of Chinese Academy of Sciences, 19A Yuquan Road, Beijing 100049, China
[c] Department of Material and Optoelectronic Science, Center of Crystal Research, National Sun Yat-Sen University, Kaohsiung 804, Taiwan
[d] School of Materials Science and Technology, Hunan Provincial Key Laboratory of Advanced Materials for New Energy Storage and Conversion, Hunan University of Science and Technology, Xiangtan 411201, China

ARTICLE INFO

Keywords:
biomass-derived nanocomposites
multifunctional
solar-to-thermal conversion
thermal management

ABSTRACT

Solar-to-thermal conversion is a direct and efficient way to –convert renewable and green sunlight to manageable thermal energy for diverse applications from steam production, energy harvest to personal thermal management. However, developing biomass-derived functional materials with eco-friendly, low-cost, and extensible features remains a challenge. Here, a cost-effective, scalable, biodegradable, and multifunctional nanocomposite was designed for solar-to-thermal applications. Through balancing the photothermal and water-absorbing capacities, the designed solar evaporator can demonstrate an efficient evaporation rate of 1.23 kg m^{-2} h^{-1} under 1 sun. Meanwhile, solar irradiation can further boost the directional water flow process, resulting in a remarkable improvement of generated voltage from the initial 410–515 mV under 1 sun. Thus, the as-prepared nanocomposites displayed an excellent comprehensive performance, which was superior to the majority of the previously reported non-biomass and other biomass materials. Furthermore, a wearable personal thermal management device was designed to simultaneously realize the electrical response of solar intensity and fast heating. As a proof of concept, a thermal managing house system enabled by solar energy was implemented to achieve an effective and eco-friendly temperature control without excessive energy consumption.

1. Introduction

The rapid depletion of fossil fuel, shortage of purified water resources, and environmental pollution/global warming have threatened sustainable development worldwide [1–3]. To address the above-mentioned challenges, renewable, clean, and mechanical energy sources can be alternatives to realize water/energy harvest [4,5]. As an inexhaustible and green source, solar energy and its related technologies have been exhaustively developed to achieve photovoltaic panels [6], thermoelectric pieces [7], solar evaporators [8–10], thermal management devices [11,12], *etc*. Among them, solar-to-thermal technology is considered as a direct, efficient, and promising candidate to absorb input sunlight and further convert it to thermal energy for interfacial water evaporation [13], thermal management [14], thermoelectric production [15,16], *etc*. The solar energy management strategy significantly depends on the modified/synthesized materials from structural design [17,18] and terminal applications [19,20]. A myriad of solar-to-thermal materials have been developed, including the plasmonic film [21], the hierarchically nanostructured gel based on polyvinyl alcohol and polypyrrole [22], the sponge-like light-absorbing hydrogel [23], organic carbon-based nanomaterials [24,25], and natural-derived sources [26]. However, the raw materials of photothermal layers still face the problems of cost, pollution potential, and scalability. Therefore, developing eco-friendly, low-cost, scalable, and accessible ways to achieve steam

* Corresponding authors at: Key Laboratory of Marine Materials and Related Technologies, Zhejiang Key Laboratory of Marine Materials and Protective Technologies, Ningbo Institute of Materials Technology and Engineering, Chinese Academy of Sciences, Zhongguan West Road 1219, Ningbo 315201, China.
E-mail addresses: xiaopeng@nimte.ac.cn (P. Xiao), tao.chen@nimte.ac.cn (T. Chen).
[1] These authors contributed equally to this work.

https://doi.org/10.1016/j.nanoen.2022.107180
Received 23 December 2021; Received in revised form 2 March 2022; Accepted 21 March 2022
Available online 24 March 2022

production, energy harvest, and integration is of great importance.

Biomass resources and their derivatives, available, renewable, biocompatible, and biodegradable features are widely used to exploit a series of solar-to-thermal materials. For example, Wu et. al. prepared the aromatic monomers by breaking the C-O or C-C bonds to achieve photocatalytic conversion of lignin and lignin-derived aromatics [27]. Gao et. al. fabricated the hybrid hydrogel evaporators by introducing the konjac glucomannan with metal-organic framework nanoparticles into the polyvinyl alcohol networks [28]. Wang et. al. built a versatile coating that can achieve solar-enabled energy management at room temperature [29]. However, due to the limited geometrical size, expensive/complicated post-treatment, difficulties in scale-up or existing non-biodegradable components, it is highly desired to develop eco-friendly, scalable, and biodegradable biomass-derived functional materials from environmental and economic perspectives for maximum energy utilization.

The 2,2,6,6-tetramethylpiperidine-1-oxyl-oxidized cellulosic NFs (TEMPO-CNFs) and melanin are widely used and abundant biomass materials [30–34]. For the critical photothermal component, the biomass-derived melanin is featured with featureless broadband absorbance ranging from UV to NIR region [35] and nonradiative dissipation of 99.9% of the captured UV and visible radiation [36], enabling a good candidate for high-efficient solar capture and conversion. Therefore, the alternative introduction of melanin can remarkably strengthen the solar-to-thermal performance. Here, we present a scalable, low-cost, and biodegradable photothermal hybrid derived from the biomass-based nanostructured nanocomposites (BBNC) of TEMPO-CNFs and melanin that coated on cellulose paper. The solar-to-thermal conversion and water-absorbing abilities of the BBNC can be adjusted by controlling the TEMPO-CNFs and melanin. The resulted photothermal BBNC can function as an efficient solar evaporator to achieve a water evaporation rate of 1.23 kg m^{-2} h^{-1} under 1 sun. Furthermore, under the evaporation-driven directional water flow, the BBNC evaporator can generate continuous electricity with voltage from the initial 410–515 mV under 1 sun. Thus, the BBNC displayed an excellent comprehensive performance, which was superior to the majority of the previously reported non-biomass and other biomass materials. Meanwhile, a wearable personal thermal management device was designed to simultaneously realize the electrical response of solar intensity and fast heating. As a proof of concept, a demo prototype was designed to achieve a solar-enabled thermal management for greenhouse system. Superior to the conventional solar-to-thermal conversion materials, the reported photothermal nanocomposites derived from biomass raw materials represent eco-friendly, biodegradable and accessible features, which can be readily extended and function as highly adaptable functional coatings for multifunctional solar energy management. The well-designed structure and integrated devices enable high-efficient utilization of the solar energy to enhanced clean water, electricity and heat harvest in a simple and effective way, demonstrating significant potentials in wide solar-to-thermal applications.

2. Experimental section

2.1. Preparation of the biomass-based nanocomposite (BBNC)

BBNC was fabricated with the suspensions of melanin and TEMPO-CNFs. The mass ratio of TEMPO-CNFs suspension (~3 mg/mL) and melanin was 6:1, 5:1, 4:1, 3:1, and 2:1. Then, the suspensions with different mass ratios were stirred for 0.5 h and ultrasound in a water bath for ~1 h. Subsequently, the TEMPO-CNFs-Melanin suspension solution was evenly coated on the cellulose paper (6.5 × 3 cm) to obtain a coating and dried at 60 °C to get the BBNC.

2.2. Preparation of the water evaporation-induced power generation device

The platinum wire electrode was fixed on one end of the BBNC with silver paste and then encapsulated with hydrophobic PDMS. After drying in the oven at 50 °C, the water evaporation-induced power generation device was obtained. The electrode integrated BBNC with a well-designed tail (1.5 ×0.5 cm) was inserted into the DI water for the directional flow process. When solar energy was applied, water evaporation was prominently enhanced to accelerate water flow velocity across the BBNC surface efficiently. The tail part of the water evaporation-induced power generation device that plays a role in water transport was inserted into the PET petri dish.

2.3. BBNC and TEMPO-CNFs film photothermal water evaporation experiment

The BBNC (1 ×1 cm) and TEMPO-CNFs film (1 ×1 cm) were placed on the top of the foam (2 ×2 cm) and floated in a beaker filled with water. A water-absorbing tail (1.5 ×0.3 cm) was designed. The solar simulator was adjusted the illuminated solar intensity ranging from 0.5 to 2 sun for water evaporation. The analytical balance was placed on the bottom and recorded mass loss date every five minutes through the analytical scale and calculating mass change (Kg m^{-2}).

2.4. The calculation of water evaporation rate (Calculate the water evaporation rate of 1 sun as an example)

The water evaporation performance experiments were conducted using a solar simulator outputting a simulated solar flux of 1 kW/m^2. The solar flux was measured using a solar power meter. The temperature was measured using an infrared thermal imager. The mass change of water was measured using a laboratory balance with 0.1 mg resolution while the steam generation was in a steady state.

2.5. BBNC water evaporation-induced power generation

Firstly, the water evaporation-induced power generation device was floated in the water. Secondly, a water-absorbing tail (1.5 ×0.3 cm) was designed to ensure water transmission and charge dissociation. Thirdly, the Pt electrodes inserted in the water and encapsulated with silver paste on the BBNC were connected to the electrochemical workstation, respectively. Finally, the voltage-time and current-time curves of the electrochemical workstation were used to record the voltage and current changes, respectively.

2.6. Solar enhanced electrical generation of BBNC photothermal water evaporation experiment

The biomass photothermal device floated in a beaker with the tail immersed into water. The electrode of BBNC connected the electrochemical workstation, which recorded the voltage data through the voltage-time curve. After the voltage remains stable, the solar simulator is used to adjust different solar intensities (0.2 sun, 0.4 sun, 0.6 sun, 0.8 sun, and 1 sun) to irradiate the surface of the biomass photothermal device and record the voltage change through the electrochemical workstation. Ensure that the voltage remains stable before each increase in solar intensity.

2.7. Synthesis of TEMPO-CNFs

TEMPO-CNFs were stripped from softwood pulp according to a typical TEMPO oxidation strategy [37,38]. Dry kraft pulp (10 g) was subjected to oxidation in a mixed solution (1 L) of TEMPO (0.04 g), NaBr (1 g), and NaClO (80–240 mmol) under alkaline conditions (pH ≈10) for 7 h fiercely stirring. After 3–5 times washing procedures with distilled

water on the Buchner funnel, the resulting flocs were homogenized in a pressure microfluidizer of 60 MPa and pH ≈ 7.0 for 3 times. The viscous product was then centrifuged at 8000 rpm to remove the aggregates and stored at 4 °C.

2.8. BBNC and TEMPO-CNFs film degradation experiment

The BBNC and TEMPO-CNFs film were soaked in natural soil leachate to assess the degradation kinetics. After a predetermined time, the samples were washed with ethanol and dried at 60 °C to weigh the mass remaining. This process was similar to biodegradation like crab chitin fully bio-based electric devices [39] and TEMPO-CNFs aerogel moisture power generation device [40].

2.9. Characterization

Transmission electron microscopy (TEM, Japan) and field emission scanning electron microscopy (FESEM, Japan) images were performed on JEOL-2100-HR (JEOL, Japan) and Hitachi-S4800 (Hitachi, Japan), respectively. The contact angle was measured using a contact angle meter (OCA-20, Germany). Ultraviolet-visible-near infrared (UV–vis–NIR) spectrophotometer (PerkinElmer, Lambda 950, USA) was used to test the transmittance and reflection of the BBNC. The IR camera (FLIR E8, Germany) was employed to realize a real-time recording of the surface temperature and IR images of the BBNC (Melanin/TEMPO-CNFs/Cellulose paper) samples. Voltage and current were recorded by an electrochemical workstation (CHI660E, China). The solar simulator (PL-X300DF, China) was used to adjust the solar intensity. A universal tensile testing machine (Zwick, Z1.0, Germany) was used to characterize the mechanical properties of the films. The analytical scale (JJ224BC, China) was used to read the film weight and water mass loss. The temperature and humidity were simultaneously recorded by a Temperature & Humidity recorder (Cos-03, China).

3. Results and discussion

3.1. Preparation scheme and characterization of the BBNC

The preparation process of the BBNC is shown in Fig. 1a. TEMPO-CNFs with negative charges was prepared through the typical TEMPO/NaClO/NaBr solution modification method [37,38,41]. Melanin is widely available from squids (Fig. 1a). The diameters of

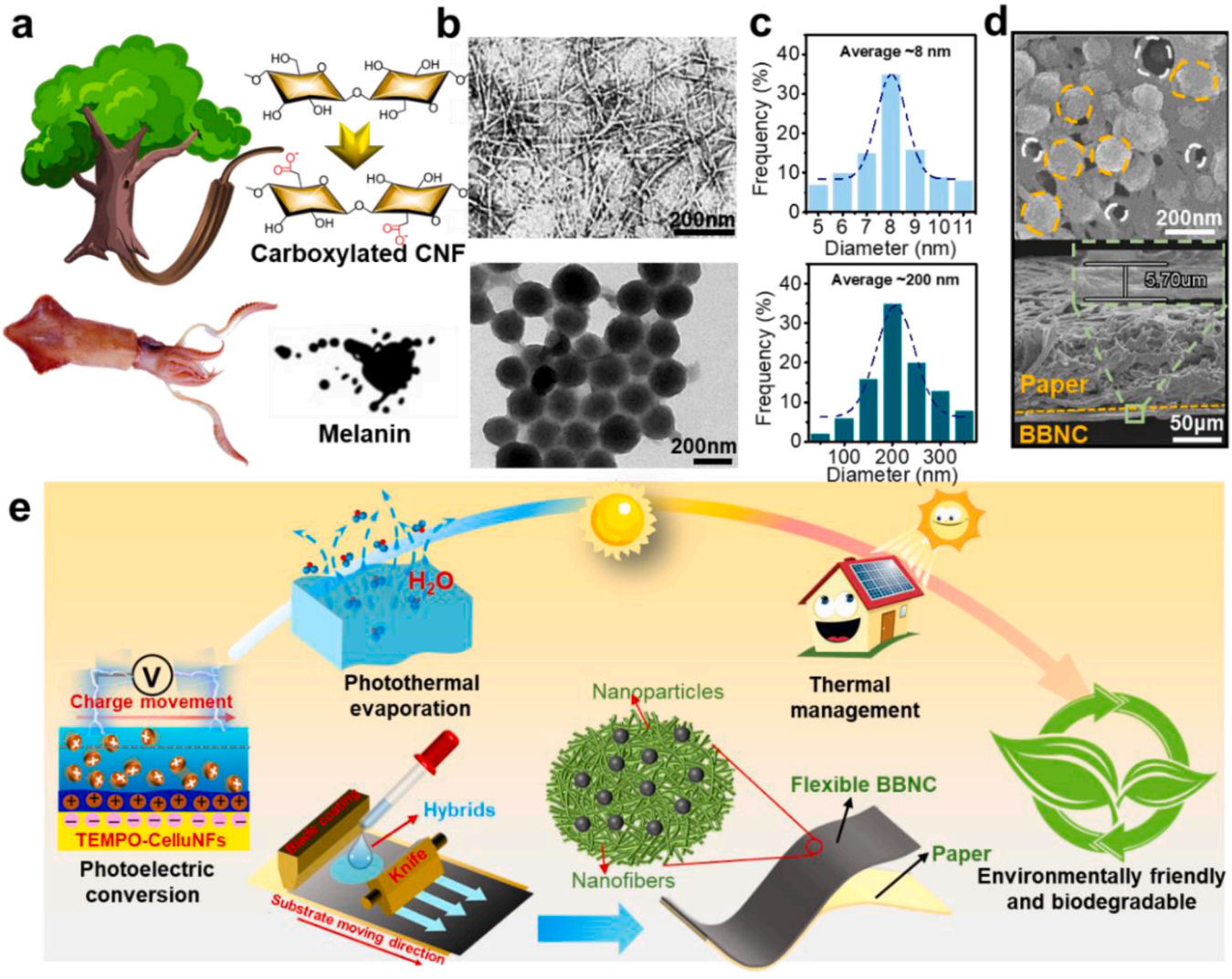

Fig. 1. Preparation and application of the biomass-derived nanostructured nanocomposites. (a) Biomass materials TEMPO-CNFs (top) and melanin (bottom) are derived from wood and squids, respectively. (b) Typical TEM image of negatively charged TEMPO-CNFs (top) and melanin nanoparticles (bottom). (c) Particle size statistics of negatively charged TEMPO-CNFs (top) and melanin nanoparticles (bottom). (d) Typical SEM image of the biomass-based nanocomposite (top: surface, bottom: cross-section). (e) Preparation and application schematic diagram of the biomass-based nanocomposite for solar-enabled multifunctional energy management.

TEMPO-CNFs and melanin nanoparticles were ~8 nm and ~200 nm, respectively (Fig. 1b and c). The TEMPO-CNFs-Melanin nanocomposites (TCC) were prepared by mixing TEMPO-CNFs and melanin's biomass materials [42–44]. The BBNC was obtained by homogeneously coating the TEMPO-CNFs-melanin nanocomposites on the cellulose paper (Fig. S1a and S1b). The detailed process flow diagram and device structure diagram is shown in Fig. S1c. SEM image clearly illustrated that hydrogen bonding embedded the melanin nanoparticles in TEMPO-CNFs (Fig. 1d). Furthermore, the resulting BBNC can take full advantage of solar energy to realize multifunctional energy management of solar-enhanced interfacial water evaporation and induced electrical generation. Besides, it can be effectively employed as a wearable thermal management device to monitor solar intensity actively and harvest thermal energy. As a proof of concept, a demo of the solar-enabled temperature control system can be achieved in a house without energy consumption. In addition, due to TEMPO-CNFs and melanin's biomass features, the BBNC was endowed with biodegradable characteristics, demonstrating significant potentials in developing environmentally friendly materials for multifunctional solar-enabled energy transformation and harvest applications (Fig. 1e).

3.2. Physical and chemical properties of the BBNC

The tensile strength of BBNC was investigated. As shown in Fig. 2a, the tensile strength of the TCC was ~25 MPa, which was higher than that of the melanin film (~5 MPa) and TEMPO-CNFs film (~12 MPa). The good physical performance of the TCC was attributed to the multiple hydrogen bond interactions between TEMPO-CNFs and melanin. Moreover, the tensile strength of BBNC can reach up to 50 MPa, which was higher than the TCC. The enhanced mechanical strength performance may result from strong combination of cellulose paper and TCC. FTIR was further carried out to evidence the interactions between TEMPO-CNFs and melanin. A strong stretching vibration peak at 1400 cm^{-1} existed in Fig. S2a. Moreover, there appeared red shift of the stretching vibration peak at 1400 cm^{-1} in the BBNC, which resulted from the hydrogen bond association between melanin and TEMPO-CNFs. In addition, From the Fig. S2b, a wide-stretching vibration absorption peak of hydrogen bond association product (carboxyl dimer O-H) at 2800–3000 cm^{-1} can be found. Furthermore, as displayed in Fig. S3, we used the thickness tester (CHY-CA, China) to test the film thickness of TEMPO-CNF, melanin, the composite coating and the resulted BBNC, respectively. And the composite coating layer showed a typical thickness of ~15 μm, which could be readily integrated onto targeted cellulose paper with the resulted BBNC thickness of ~150 μm. In addition, the BBNC endowed excellent flexibility and mechanical stability to be easily cut to diverse shapes for considerable solar-to-thermal conversion capability (Fig. 2b). Meanwhile, the wettability of the BBNC was also crucial for further applications of water evaporation and electrical generation. The contact angle measurement illustrated the water droplet could be fully absorbed into the BBNC within 8 s (Fig. 2c).

The biodegradability of the BBNC was further studied. The degradation process was carried out as following steps. Firstly, the soil leachate penetrated the film and increased film volume and swelling. Secondly, the film oozed out its substance to fully contact the

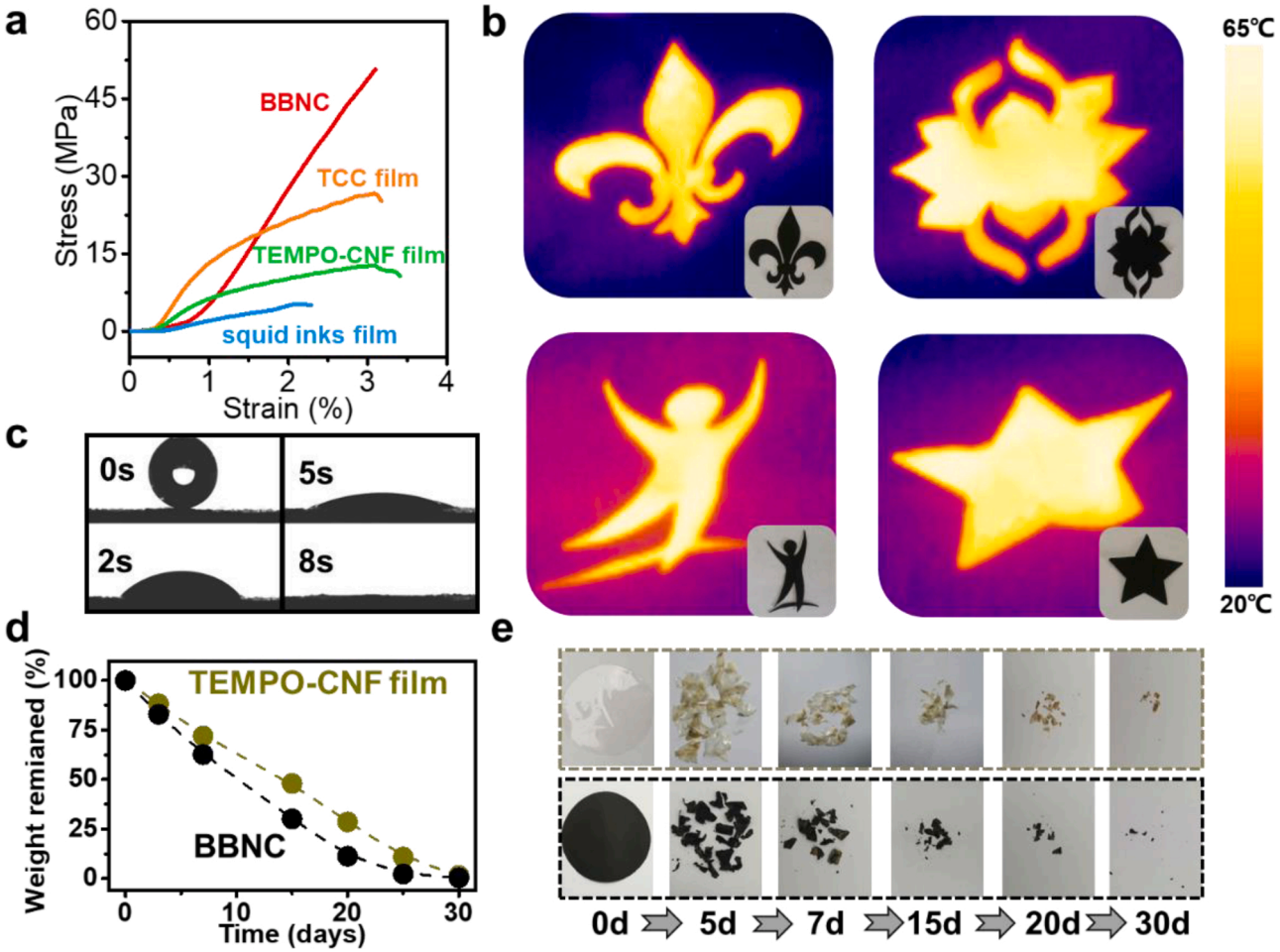

Fig. 2. Physical and chemical properties of the BBNC. (a) The stress-strain curves of BBNC, TCC, TEMPO-CNFs and melanin films, respectively. (b) IR images and optical picture of BBNC cut into different shapes. (c) Contact angle of BBNC. (d) The weight loss and (e) optical image of TEMPO-CNFs film and BBNC degradation in soil for different periods.

microorganisms (bacteria and mildew) in the soil leachate. Thirdly, under the action of microbial activity, the enzyme entered the active site of the polymer and penetrated the point of action of the polymer to break the polymer molecular skeleton into small segments. Lastly, the molecular weight gradually decreased and became a monomer that was swallowed by microorganisms. It was wholly metabolized into carbon dioxide and water to complete the degradation process [45]. As shown in Fig. 2d and e, the BBNC can be fully degraded in natural soil leachate within 30 days, indicating its excellent biodegradability.

3.3. *The water evaporation-induced power generation of the BNNC and optimization*

The water evaporation-induced power generation performance of the BNNC was further studied by loading charges and controlling capillary pores to enable adequate directional water flow for electrical generation. The mechanism of the water evaporation-induced power generation device of BBNC was shown in Fig. S4. When water molecules were contacted with the BBNC, the overlapped electric double layer (EDL) spontaneously formed at the solid (TEMPO-CNFs)-liquid (DI Water) interface with a size comparable to the Debye length [46] (Fig. 3a). In our study, TEMPO-CNFs in the BBNC contained sufficient dissociable polar groups (-COOH and -COONa) that the zeta potential was ≈−48.3 mV at pH= 7 (Fig. S5). This process results in a flowing current and a streaming potential [40,47]. Furthermore, the voltage remained relatively stable under ambient conditions in our tests (T ≈ 25 °C, RH≈51%).

More importantly, the concentration of TEMPO-CNFs also played a significant role in the power generation performance of the BBNC. As shown in Fig. 3b, when the concentration of TEMPO-CNFs was 3 mg/mL, the voltage (V) and current (I) values of the BBNC reached the maximum at 410 mV and 150 nA, respectively. In this case, the maximum output power was 63 nW (Fig. S6). When the concentration of TEMPO-CNFs increased from 1 to 3 mg/mL, the carboxyl content remarkably increased. Therefore, the dissociation charges, V and I of the BBNC increased (Figs. S7 and S8). Moreover, when the concentration of the TEMPO-CNFs was above 3 mg/mL, the TEMPO-CNFs solution had an undesirable higher viscosity, resulting in the inhomogeneous coating

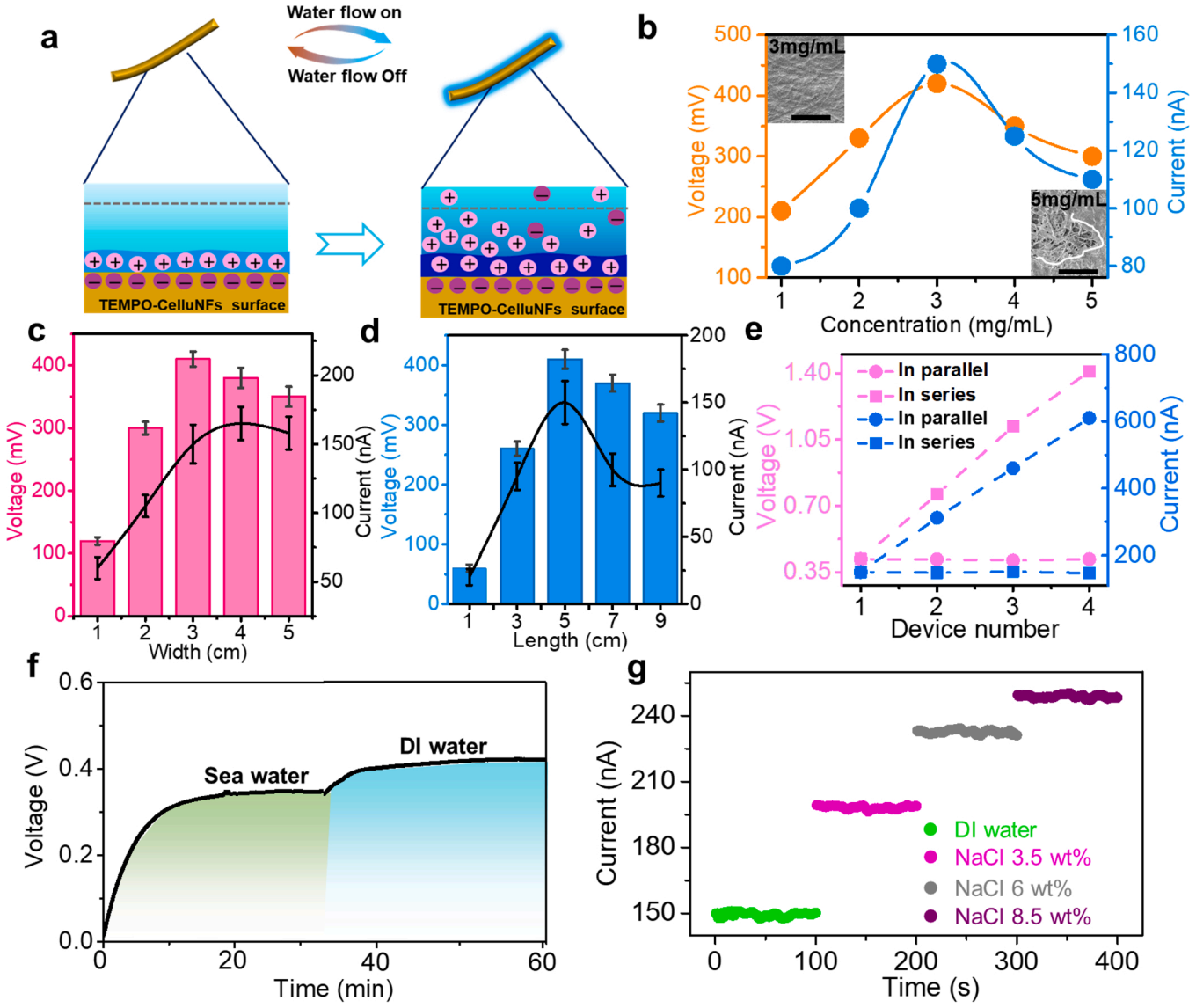

Fig. 3. Water evaporation-induced power generation mechanism and shapes optimization of the device of BBNC. (a) Schematic diagram of the voltage caused by the directional movement of free ions in the hydrated charged nanochannel and the difference in ion concentration. (b) Effect of TEMPO-CNFs concentration on V and I. (c–d) Effect of length and width of the biomass-based nanocomposite on V and I. (e) V and I of energy conversion devices in series and parallel (f-g) Effect of electrolyte concentration on V and I. Device length: 5 cm; width: 3 cm; Thickness: ~150 μm.

on the paper surface and reduced water evaporation-induced power generation performance of the BBNC (Fig. 3b and Fig. S9).

Apart from this, the voltage and current value can also be tuned by changing the aspect ratio of the BBNC (Fig. S10). As shown in Fig. 3c and d, the optimal length-width ratio of BBNC was 5 cm and 3 cm. In this case, the maximum voltage and the current value can be achieved at ~410 mV and ~150 nA, respectively. Furthermore, the coating thickness also impacted power generation performance. We control the coating thickness to explore the effect of thickness on the performance. According to Fig. S11a, the two-layers coating of BBNC was optimal with a voltage as high as ~0.48 V. In this case, we further achieved an optimal power value of 87 nW with a voltage of ~0.48 V and current of ~180 nA (Fig. S11b)." In addition, the BBNC could be further connected in series or parallel style for a higher value of voltage or current (Fig. 3e and Fig. S12).

The species of liquid electrolytes were also controlled to explore the electrical performance of the integrated BBNC. The integrated device was transferred to simulated "seawater" (3.5 wt% NaCl solution) when the water voltage remained stable. Due to the increase of electrolyte concentration, the generated voltage reduced from ~0.41 to ~0.34 V (Fig. 3f). However, the current can experience a similar increasing trend with the increase of the NaCl solution electrolyte concentration from 3.5 to 8.5 wt% (Fig. 3g and S13). To further evidence the universality of this strategy, a series of other biomass-derived materials (e.g., carboxymethylcellulose sodium, sodium alginate, chitosan and tannic acid) were acquired to mix with melanin for photothermal coating. The result showed that all the achieved biomass-based coatings demonstrated favorable power generation performance (Fig. S14).

3.4. Proportion optimization of BBNC

The effect of the mass ratios of TEMPO-CNFs and melanin on the topography of the BBNC was surveyed. As shown in Fig. S15, the color of BBNC presented a gradually decreased tendency when the mass ratios of TEMPO-CNFs and melanin increased from 2:1, 3:1, 4:1, 5:1, 6:1, to 1:0. Moreover, there was a remarkable micromorphology difference of BBNC with the increased mass ratios of TEMPO-CNFs and melanin. As shown in Fig. 4a, the microstructures of the BBNC surface demonstrated a transition from rough to smooth morphology. Furthermore, the effect of the mass ratio of melanin to TEMPO-CNFs on the evaporation and electrical production performance of the BBNC was explored to acquire an optimal mass ratio of BBNC. When the relative proportion of melanin was 2:1 and 3:1, the solar absorption and photothermal evaporation rates showed a higher value (Fig. 4b and c). However, the excessive melanin nanoparticles could gather on the cellulose nanofibers, which can severely prevent the effective transportation of water molecules and ions across cellulose nanofibers' surface, thus bringing a declined power generation (Fig. 4a and c).

Moreover, from the Fig. S16, we can further understand that the proportion of CNF reduction will lead to a decrease in the water absorption and water absorption rate of BBNC. The low content of TEMPO-CNFs could bring out the reduced dissociation charges, which could also minimize the electrical production performance of the BBNC. As to the low content of the melanin, such as 5:1 and 6:1 in the BBNC, the evaporation ability of the BBNC reduced and the generated power performance-enhanced (Figs. 4c and S17–S19). Therefore, the most suitable proportion of the TEMPO-CNFs and melanin was 4:1 through the consideration of solar thermal evaporation and electrical production performance. In this condonation, the maximum power production performance of the BBNC was the voltage of ~410 mV and the current of ~150 nA. In addition, the maximum water evaporation rate of the BBNC was ~1.23 kg m^{-2} h^{-1}.

3.5. Photothermal performance of the BBNC

The evaporation performance of BBNC was further investigated. The

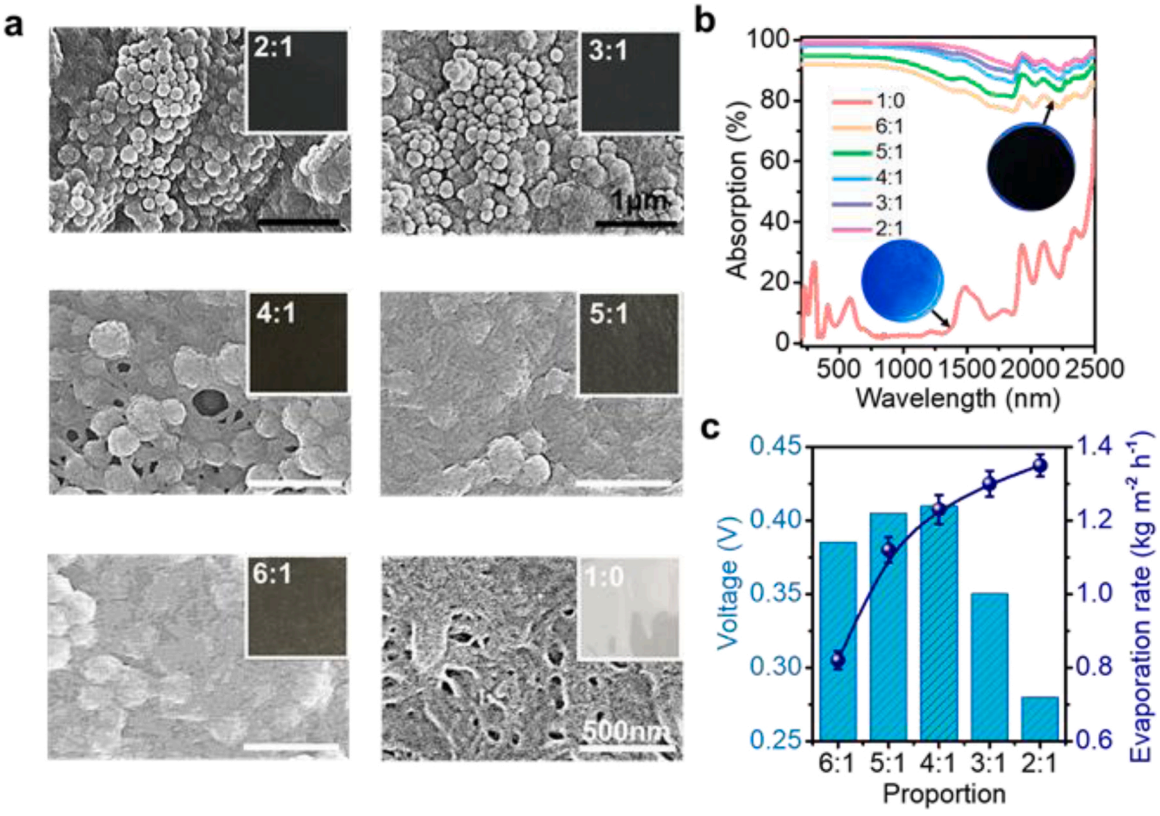

Fig. 4. Melanin proportion optimization and characterization of the BBNC. (a–b) SEM images and absorption of the BBNC at different proportions of TEMPO-CNFs and melanin. (c) Voltage and evaporation rate of the BBNC at different proportions of TEMPO-CNFs and melanin.

absorbance of BBNC (mass ratio: TEMPO-CNFs/melanin=4:1) in the visible light band was 97% (Fig. 4b). Therefore, the BBNC can absorb solar energy and increase its surface temperature under sufficient sunlight. A simulated solar (1 kW/m^2) was applied to characterize the solar-to-thermal conversion capability of the BBNC. The BBNC showed a remarkable temperature elevation measured by IR camera (Fig. 5a). Owing to the introduction of melanin, the maximum temperature of BBNC can reach up to 42 °C after 6 min. In contrast, the temperature of the TEMPO-CNFs film and pure water can only attain ~29 °C and ~23.5 °C, respectively (Figs. 5b and S20). The increasing temperature of BBNC can promote rapid water evaporation to achieve photothermal evaporation [28,48,49]. The BBNC with a water-absorbing tail was designed, as shown in Fig. 5c. The illuminated solar intensity was adjusted from 0.5 to 2 sun for water evaporation. It can be found that the evaporation rates of BBNC were proportional was the solar power (Fig. 5d and e). Under the irradiation of the 1 sun and 2 suns, the maximum evaporation rates of the BBNC were 1.23 kg m^{-2} h^{-1} and 2.01 kg m^{-2} h^{-1}, respectively (Fig. 5e). In addition, as shown in Fig. S21, we prepared BBNC tails with different sizes and tested the corresponding photothermal evaporation performance under one sun. We can find that the photothermal evaporation rate of the BBNCs with different tail sizes shows a similar value of ~1.2 kg m^{-2} h^{-1}, demonstrating that the sizes of tails cannot remarkably affect the final photothermal evaporation performance. The reason may result from the completely immersed forms of the tails, which can contribute little to the effective evaporative areas.

3.6. Solar enhanced electrical generation performance

Since solar intensity can remarkably enhance water evaporation, the performance of electrical generation enabled by evaporation-induced water flow is expected to be elevated with the introduction of solar energy. The mechanism of the solar enhanced gradient power generation system was illustrated in Figs. S4a and 4b. Under solar irradiation, the BBNC concentrated solar heating and induced a high temperature, so the vapour was generated at the surface. The water was transported to the surface to maintain the sustainable evaporation by capillary force in the BBNC through a designed tail structure (Fig. S4b) [50]. Due to the rich carboxyl groups in TEMPO-CNFs, large amounts of Na^+ and H^+ dissociated on nanofiber surface. Therefore, as shown in Fig. S22, the rapid water evaporation of the BBNC induced a high ion concentration difference between the tail and top electrode [40], which can be applied to produce electricity. Also, the increasing solar intensity can accelerate the water evaporation and ion dissociation on the surface of the nanofibers, increasing the ion concentration difference and increasing the voltage. Finally, the generated voltage can gradually reach a stable value [3]. Since the water evaporation mainly depends on the heat exchange under the circumstance of fixed wind speed and evaporative areas, we further explored the effect of photocurrent on the performance of photothermal water evaporation. Actually, the power generator is similar to the primary cell. When the cell worked, it could both output energy and also generate heat inside itself. To further investigate the abovementioned factors, the corresponding control experiments were conducted. In our system, the conventional solar evaporator was conventional in the form of open circuit (Fig. S23a), which could serve as the control with no photocurrent applied. On the other hand, as shown in Fig. S23b, for the form of closed circuit of BBNC-based solar evaporator, two Pt electrodes inserted in the water and encapsulated with silver paste on the BBNC were both connected to the capacitor. In this case, a typical photocurrent can be effectively generated and the BBNC-based evaporator is powered by the capacitor with electrothermal energy generated in closed circuit. However, it was observed that the BBNC-based evaporator in the form of open and closed circuit represented the typical evaporation rates of ~1.23 kg m^{-2} h^{-1} and ~1.25 kg m^{-2} h^{-1}, respectively (Fig. S23c). Ideally, the generated power can be further employed to generate heat and accelerate the

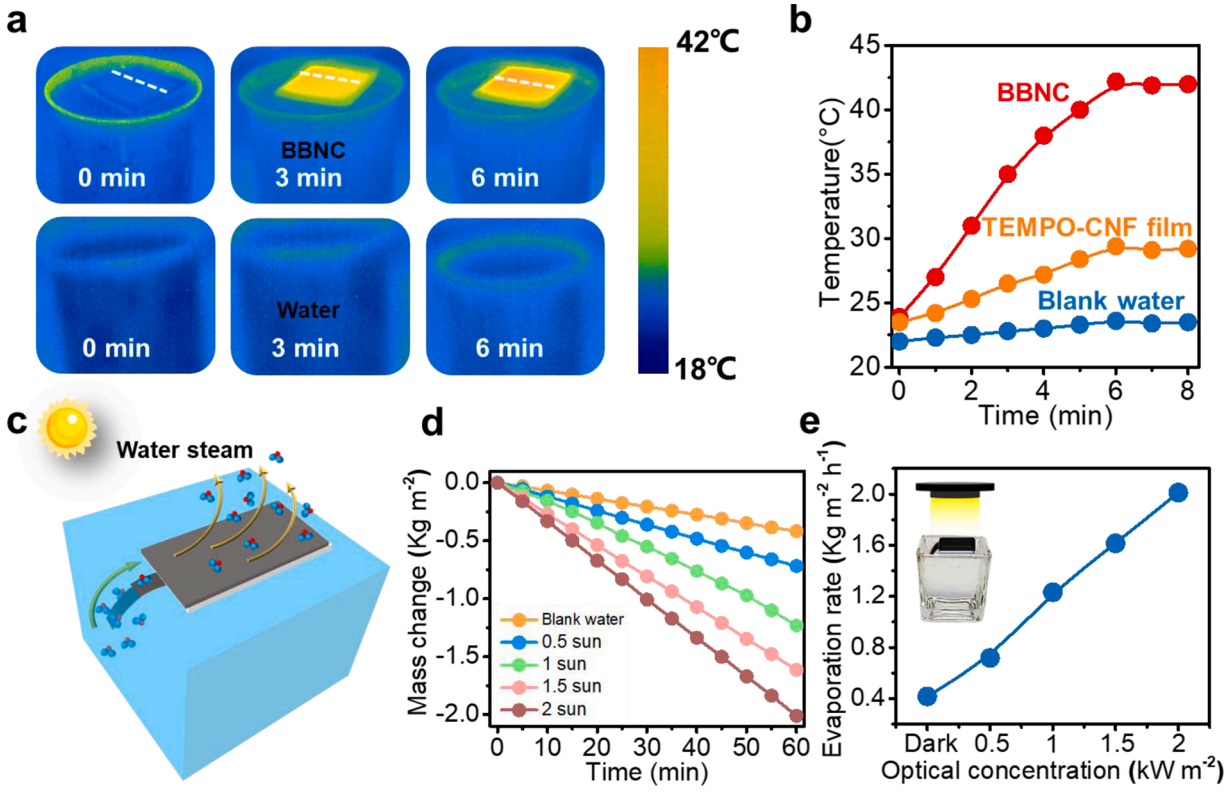

Fig. 5. Photothermal conversion performance of the BBNC. (a) IR images of pure water and BBNC under 1 sun. (b) Temperature versus time curves of pure water, TEMPO-CNFs film, and BBNC. (c) The photothermal conversion schematic of the BBNC. (d-e) The mass change and evaporation rate of the BBNC under different solar irradiation.

evaporation rate. However, owing to the relatively low power at the level of nW, the electrical-thermal conversion can contribute little to the resulted evaporation performance.

The solar enhanced electrical generation performance of the BBNC was comprehensively studied. As illustrated in Fig S24, when solar illumination was applied, the strengthened evaporation rate of the water and flow velocity (v) can prominently increase the unit flux and flow rate of hydronium ions. It can be known from the Streaming potential (V_{Str}) Smoluchowski equation [51].

$$V_{Str} \approx \frac{\tau\alpha}{(\mathbb{C}+\gamma)\mu} v$$

where τ is the zeta potential of the charged surface, α is the hydraulic flow resistance, $\mathbb{C}$ is ionic concentration, γ is the offset concentration, μ is the effective ionic mobility, and v is the flow velocity. Therefore, this process will result in a greater streaming current and create a higher potential [52]. Moreover, the effect of greater streaming current/potential can enhance the power output. Therefore, the introduction of solar energy can lead to remarkably enhanced streaming potential to improve the resulted electrical performance of BBNC. Based on this potential mechanism, the original balance of the power generation can be transformed to a new one, demonstrating a solar-enhanced power generation performance. As shown in Fig. 6a, the photovoltage presented a gradual increase tendency from 410 mV to 515 mV when the solar intensity increased from 0.2 sun to 1.0 sun. Moreover, the evaporation rate of the BBNC reached to 1.23 kg m^{-2} h^{-1} under 1 sun. Therefore, the BBNC presented favorable solar-enhanced power generation and water purification performance under 1.0 sun, which was comparable to the majority of the previously reported non-biomass and other biomass materials (Table S1). In addition, the electrolyte concentration also plays an important role on the performance of the generated photocurrent. As shown in Fig. S25, in the absence of electrolyte, there existed streaming potentials. In this case, the photovoltage and photocurrent are ~0.515 V (V_1) and ~180 nA (I_1), respectively, under one sun (Fig. S26). When the electrolyte is introduced into this system, the rapid evaporation of water on the surface of the BBNC will further create a higher ions concentration ($\mathbb{C}$). The ions power can be utilized to produce electricity. This process results in a higher streaming current and lower potential. In this case, the photovoltage and photocurrent are ~0.42 V (V_2) and ~200 nA (I_2), respectively, under one sun (Fig. S26).

Furthermore, the BBNC showed long-term stability of the photothermal evaporation rate and water evaporation-induced power generation performance. As shown in Figs. 6b and Fig. S27a, the voltage value and light-heat evaporation rate of the BBNC maintained their initial 410 mV and ~1.23 kg m^{-2} h^{-1} for 24 h, respectively. In addition, the gradient power generation performance of the BBNC was above 350 mV even after five days (Fig. S27b). This excellent performance was due to water transport, and ion dissociation remained constant (e.g., H^+, Na^+ ions) during the continuous evaporation. The stable solar enhanced electrical generation performance of the BBNC makes it possible for convenient accumulation and storage of electricity. Based on this, a commercial capacitor with a capacitance of 45 μF was charged for ~24 h with the prepared BBNC and further employed as a power supply for daily electrical appliances. As displayed in Fig. 6b and c, the capacitor can be power the LEDs with different colors, and the children's electronic watches with a rated voltage of 1.5 V.

3.7. Thermal response and thermal management performance

More interestingly, the editable BBNC can function as a wearable thermal management device, which can effectively capture the solar light and then convert it to considerable thermal energy. Based on the bilayer structure of the wearable device, the thermal energy was further transported to the cellulose paper layer and indirectly heated the skin (Fig. 7a). Under 1 sun illumination, the surface temperature of the BBNC-based device experienced a remarkable improvement from 30° to 62°C (Fig. 7b). Note that the thermal management device can interact with the skin in a contact way, enabling a direct contact between the pure cellulose paper side and skin surface. As illustrated in Fig. 7a, the

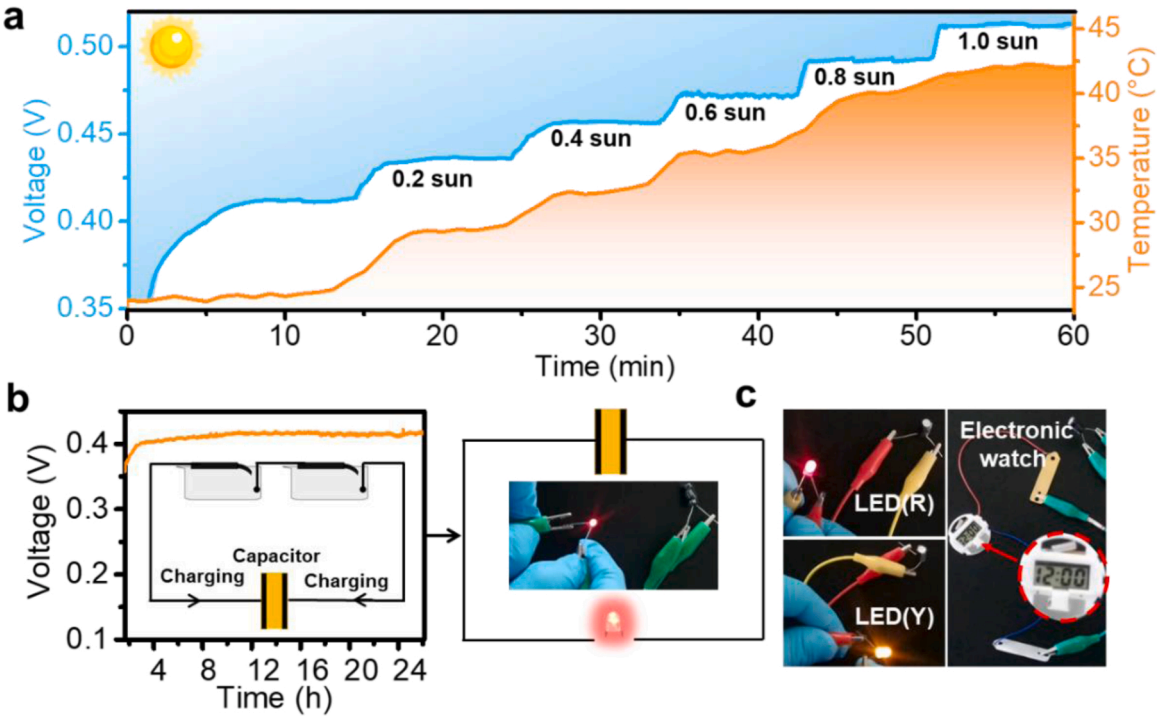

Fig. 6. Application of the BBNC for solar enhanced electrical generation performance. (a) Voltage and temperature of BBNC under a series of solar irradiation ranging from 0.2 sun to 1.0 sun. (b) Long-term continuous discharging curve (Left) of commercial capacitors with energy conversion devices and commercial red LED powered by capacitors (Right). (c) Different color LED and electronic watch powered by capacitors.

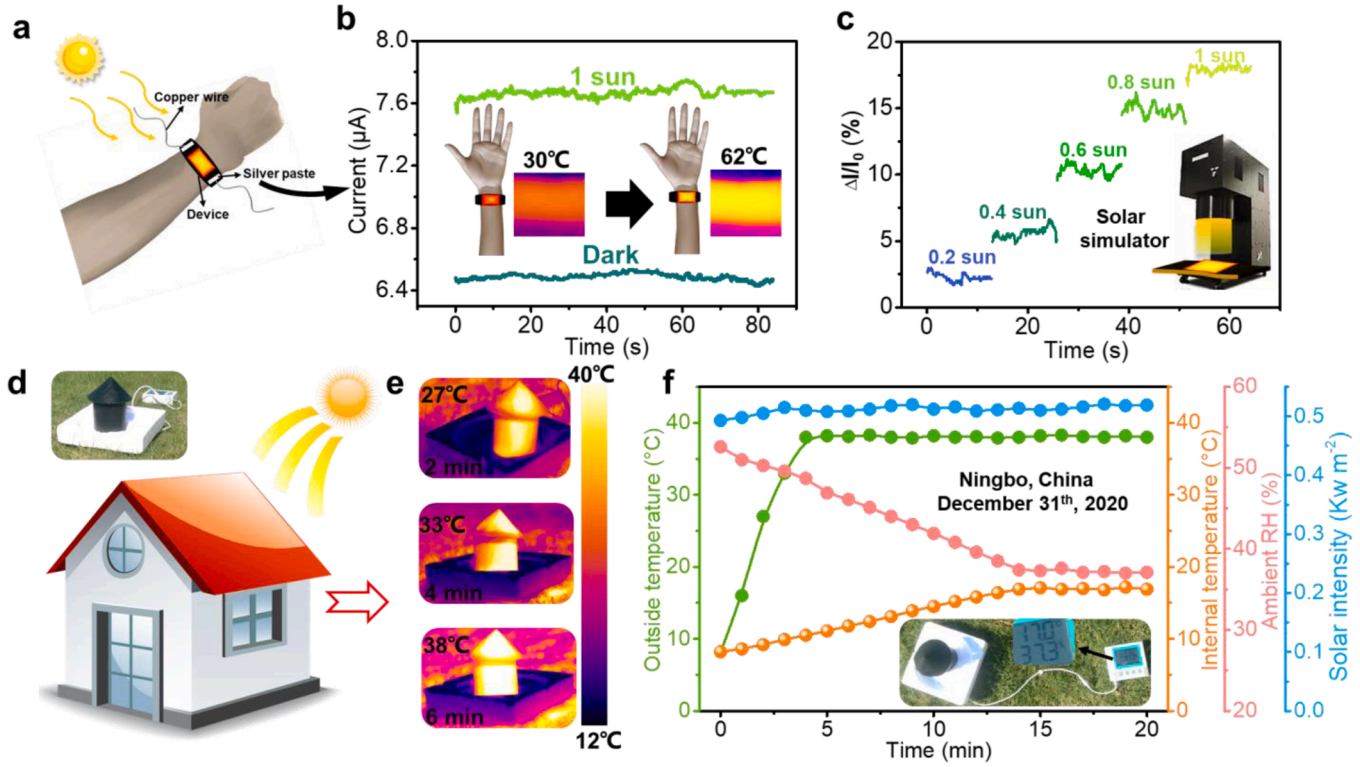

Fig. 7. Thermal response and thermal management performance of the BBNC. (a) Schematic diagram of BBNC-based wearable thermal response device. (b) Current thermal response curve of BBNC. (c) Relative current change of the BBNC as a series of solar irradiation ranging from 0.2 sun to 1.0 sun. (d) Schematic diagram of thermal management that simulates solar irradiating a house. (e) Thermal imaging temperature variation changes of the "BBNC house" in three minutes. (f) "Indoor" and "outdoor" temperature variation when exposed to solar radiation at natural conditions (Beijing Time 12:00–12:30, Ningbo in South China, Daytime on Dec. 31th, 2020). BBNC "insulated house" diameter: 10 cm; Height: 15 cm.

BBNC was cut into a long strip and further attached to the skin for wearable paper-based thermal management device. Two copper wires were fixed at the two electrodes using silver paste for thermal response test. In detail, the BBNC can effectively absorb the solar input and further convert it into considerable thermal energy. The generated thermal energy can be further transported and indirectly heat the skin via an infrared irradiation way (Fig. S28a). Therefore, the considerable heat can be effectively acquired in the potential form of by heat conduction, convection and heat radiation. Note that conduction loss of external components in our system is neglected [53,54]. As a result, although the surface temperature of the BBNC film is ~62 °C, the temperature transmitted to the skin through thermal radiation was only ~37 °C, which would not burn the human skin (Fig. S29). In addition, the absorbed solar energy can effectively power the outer electrons of BBNC to break free from the bondage of their nuclei for the formation of free electrons, resulting in an elevation of conductivity. Fig. 7b clearly illustrates that the sunlight (1 kW/m^2) could affect the original current prominently from 6.5 ~μA to 7.7 ~μA. Furthermore, a series of solar intensity (0.2, 0.4, 0.6, 0.8, and 1 sun) was selected to explore the response capability of BBNC. The result demonstrated that the current was positively correlated with the applied solar intensity (Fig. 7c). In addition, even under the irradiation of 1 sun, the current change rate can reach ~18.2%. Therefore, the BBNC is expected to be a solar detector via the current change.

Moreover, owing to the prominent solar-to-thermal property of BBNC, a proof of concept, a house model entirely composed of BBNC with a solar-enable temperature control system was designed (Fig. 7d). The BBNC-based house model can effectively receive the solar input and generate considerable temperature through efficient solar-to-thermal conversion. Furthermore, the generated thermal energy can be further transported to the cellulose paper layer, which can indirectly heat the inner room via infrared radiation (see details mechanism in the Fig. S28b.). Due to the outstanding solar absorption of the BBNC, the outdoor temperature of the house increased from 7 °C to 38 °C within 3 mins (Fig. 7e). As displayed in Fig. 7f, the indoor and outdoor temperature was collected (Dec. 31th, 2020, Ningbo in South China: East longitude ~121°and North latitude ~29°).

4. Conclusion

In summary, a low-cost, scalable, and biodegradable BBNC was developed for multifunctional solar-enabled energy management by taking advantage of cellulose nanofibers and melanin hybrids. Due to the introduction of melanin, the as-prepared BBNC can function as a solar evaporator to achieve an efficient evaporation rate of 1.23 kg m^{-2} h^{-1} under 1 sun. Moreover, the BBNC presented an excellent solar enhanced electrical generation performance under the synergy of melanin and the TEMPO-CNFs with rich carboxyl groups. Thus, the BBNC displayed an excellent comprehensive performance under 1.0 sun, which was superior to the majority of the previously reported non-biomass and other biomass materials. Therefore, the obtained BBNC can be used as a wearable thermal management device, integrated with the electrical response of solar intensity and heating functions. Benefiting from this, an integrated thermal managing house system and control the room temperature driven by sunlight in an energy-free way can be achieved by using the obtained BBNC.

CRediT authorship contribution statement

Weiqing Yang and **Peng Xiao:** Methodology, Validation, Writing – review & editing. **Tao Chen:** Reviewing, Supervision and Funding acquisition. **Chang Zhang** and **Feng Ni:** Data curation and Visualization. **Jincui Gu**, **Shiao-Wei Kuo** and **Qingquan Liu:** Investigation and Data curation and Writing – original draft.

Declaration of Competing Interest

The authors declare that they have no known competing financial interests or personal relationships that could have appeared to influence the work reported in this paper.

Acknowledgments

This research was supported by the Natural Science Foundation of China (52073295), the Sino-German Mobility Program (M-0424), Ningbo Public Welfare Science and Technology Plan Project (2021S150), Ningbo Science and Technology Bureau (2021Z127), Key Research Program of Frontier Sciences, Chinese Academy of Sciences (QYZDB-SSWSLH036), Bureau of International Cooperation, Chinese Academy of Sciences (174433KYSB20170061), and K. C. Wong Education Foundation (GJTD-2019-13).

Appendix A. Supporting information

Supplementary data associated with this article can be found in the online version at doi:10.1016/j.nanoen.2022.107180.

References

[1] M.A. Shannon, P.W. Bohn, M. Elimelech, J.G. Georgiadis, B.J. Marinas, A. M. Mayes, Science and technology for water purification in the coming decades, Nature 452 (2008) 301–310.
[2] W. Liu, Z. Wang, G. Wang, G. Liu, J. Chen, X. Pu, Y. Xi, X. Wang, H. Guo, C. Hu, Z. Wang, Integrated charge excitation triboelectric nanogenerator, Nat. Commun. 10 (2019) 1426.
[3] G. Xue, Y. Xu, T. Ding, J. Li, J. Yin, W. Fei, Y. Cao, J. Yu, L. Yuan, L. Gong, J. Chen, S. Deng, J. Zhou, W. Guo, Water-evaporation-induced electricity with nanostructured carbon materials, Nat. Nanotechnol. 12 (2017) 317–321.
[4] M. Ejeian, R. Wang, Adsorption-based atmospheric water harvesting, Joule 5 (2021) 1678–1703.
[5] F. Kucherov, E. Gordeev, A. Kashin, V. Ananikov, Three-dimensional printing with biomass-derived PEF for carbon-neutral manufacturing, Angew. Chem. Int. Ed. 56 (2017) 15931–15935.
[6] F. Bonaccorso, L. Colombo, G. Yu, M. Stoller, V. Tozzini, A. Ferrari, R. Ruoff, V. Pellegrini, 2D materials Graphene, related two-dimensional crystals, and hybrid systems for energy conversion and storage, Science 347 (2015), 1246501.
[7] Y. Zhong, Li Zhang, V. Linseis, B. Qin, W. Chen, L. Zhao, H. Zhu, High-quality textured SnSe thin films for self-powered, rapid-response photothermoelectric application, Nano Energy 72 (2020), 104742.
[8] Y. Zhang, L. Wu, X. Wang, J. Yu, B. Ding, Super hygroscopic nanofibrous membrane-based moisture pump for solar-driven indoor dehumidification, Nat. Commun. 11 (2020) 3302.
[9] Y. Yang, R. Zhao, T. Zhang, T. Zhao, P. Xiao, Y. Ma, P. Ajayan, G. Shi, Y. Chen, Graphene-based standalone solar energy converter for water desalination and purification, ACS Nano 12 (2018) 829–835.
[10] L. Cui, P. Zhang, Y. Xiao, Y. Liang, H. Liang, Z. Cheng, L. Qu, High rate production of clean water based on the combined photo-electro-thermal effect of graphene architecture, Adv. Mater. 30 (2018), 1706805.
[11] P. Hsu, A. Song, P. Catrysse, C. Liu, Y. Peng, J. Xie, S. Fan, Y. Cui, Radiative human body cooling by nanoporous polyethylene textile, Science 353 (2016) 1019–1023.
[12] A. Leroy, B. Bhatia, C. Kelsall, A. Castillejo-Cuberos, L. Zhao, L. Zhang, A. Guzman, E. Wang, High-performance subambient radiative cooling enabled by optically selective and thermally insulating polyethylene aerogel, Sci. Adv. 5 (2019), eaat9480.
[13] M. Zou, Y. Zhang, Z. Cai, C. Li, Z. Sun, C. Yu, Z. Dong, L. Wu, Y. Song, 3D printing a biomimetic bridge-arch solar evaporator for eliminating salt accumulation with desalination and agricultural applications, Adv. Mater. 33 (2021), 2102443.
[14] Y. Fang, X. Zhao, G. Chen, T. Tat, J. Chen, Smart polyethylene textiles for radiative and evaporative cooling, Joule 5 (2021) 752–754.
[15] W. Dai, W. Liu, J. Yang, C. Xu, A. Alabastri, C. Liu, P. Nordlander, Z. Guan, H. Xu, Light Sci. Appl. 120 (2020) 2047–7538.
[16] P. Xiao, J. He, F. Ni, C. Zhang, Y. Liang, W. Zhou, J. Gu, J. Xia, S. Kuo, T. Chen, Exploring interface confined water flow and evaporation enables solar-thermal-electro integration towards clean water and electricity harvest via asymmetric functionalization strategy, Nano Energy 68 (2020), 104385.
[17] S. Chaule, J. Hwang, S. Ha, J. Kang, J. Yoon, J. Jang, Rational design of a high performance and robust solar evaporator via 3D-printing technology, Adv. Mater. 33 (2021), 2102649.
[18] Z. Wang, X. Wu, F. He, S. Peng, Y. Li, Confinement capillarity of thin coating for boosting solar-driven water evaporation, Adv. Funct. Mater. 31 (2021), 2011114.
[19] Y. Zhu, G. Tian, Y. Liu, H. Li, P. Zhang, L. Zhan, R. Gao, C. Huang, Low-cost, unsinkable, and highly efficient solar evaporators based on coating MWCNTs on nonwovens with unidirectional water-transfer, Adv. Sci. 8 (2021), 2101727.
[20] H. Li, W. Zhu, M. Li, Y. Li, R. Kwok, J. Lam, L. Wang, D. Wang, B. Tang, Side area-assisted 3D evaporator with antibiofouling function for ultra-efficient solar steam generation, Adv. Mater. 33 (2021), 2102258.
[21] Y. Liu, S. Yu, R. Feng, A. Bernard, Y. Liu, Y. Zhang, H. Duan, W. Shang, P. Tao, C. Song, T. Deng, A bioinspired, reusable, paper-based system for high-performance large-scale evaporation, Adv. Mater. 27 (2015) 2768–2774.
[22] F. Zhao, X. Zhou, Y. Shi, X. Qian, M. Alexander, X. Zhao, S. Mendez, R. Yang, L. Qu, G. Yu, Highly efficient solar vapour generation via hierarchically nanostructured gels, Nat. Nanotechnol. 13 (2018) 489–495.
[23] Y. Guo, X. Zhou, F. Zhao, J. Bae, B. Rosenberger, G. Yu, Synergistic energy nanoconfinement and water activation in hydrogels for efficient solar water desalination, ACS Nano 13 (2019) 7913–7919.
[24] S. Tu, L. Xu, J. El-Demellawi, H. Liang, X. Xu, S. Lopatin, S. Wolf, X. Zhang, H. Alshareef, Autonomous MXene-PVDF actuator for flexible solar trackers, Nano Energy 77 (2020), 105277.
[25] P. Zhang, J. Li, L. Lv, Y. Zhao, L. Qu, Vertically aligned graphene sheets membrane for highly efficient solar thermal generation of clean water, ACS Nano 11 (2017) 5087–5093.
[26] H. Liu, C. Chen, G. Chen, Y. Kuang, X. Zhao, J. Song, C. Jia, X. Xu, E. Hitz, H. Xie, S. Wang, F. Jiang, T. Li, Y. Li, A. Gong, R. Yang, S. Das, L. Hu, High-performance solar steam device with layered channels: artificial tree with a reversed design, Adv. Energy Mater. 8 (2018), 1701616.
[27] X. Wu, N. Luo, S. Xie, H. Zhang, Y. Wang, Photocatalytic transformations of lignocellulosic biomass into chemicals, Chem. Soc. Rev. 49 (2020) 6198–6223.
[28] Y. Guo, H. Lu, F. Zhao, X. Zhou, W. Shi, G. Yu, Biomass-derived hybrid hydrogel evaporators for cost-effective solar water purification, Adv. Mater. 32 (2020), 1907061.
[29] Z. Wang, M. Han, F. He, S. Peng, Y. Li, Versatile coating with multifunctional performance for solar steam generation, Nano Energy 74 (2020), 104886.
[30] X. Li, M. Li, J. Xu, J. You, Z. Yang, C. Li, Evaporation-induced sintering of liquid metal droplets with biological nanofibrils for flexible conductivity and responsive actuation, Nat. Commun. 10 (2019) 3514.
[31] J. Zhou, W. Liu, X. Zhao, Y. Xian, W. Wu, X. Zhang, N. Zhao, F. Xu, C. Wang, Natural melanin/alginate hydrogels achieve cardiac repair through ROS scavenging and macrophage polarization, Adv. Sci. 8 (2021), 2100505.
[32] H. Qin, Y. Zhang, J. Jiang, L. Wang, M. Song, R. Bi, P. Zhu, F. Jiang, Multifunctional superelastic cellulose nanofibrils aerogel by dual ice-templating assembly, Adv. Funct. Mater. 31 (2021), 2106269.
[33] Z. Zeng, T. Wu, D. Han, Q. Ren, G. Siqueira, G. Nystrom, Ultralight, flexible, and biomimetic nanocellulose/silver nanowire aerogels for electromagnetic interference shielding, ACS Nano 14 (2020) 2927–2938.
[34] W. Zhang, X. Wang, Y. Zhang, B. Bochove, E. Mäkiläc, J. Seppälä, W. Xua, S. Willför, C. Xu, Robust shape-retaining nanocellulose-based aerogels decorated with silver nanoparticles for fast continuous catalytic discoloration of organic dyes, Sep. Purif. Technol. 242 (2020), 116523.
[35] P. Meredith, T. Sarna, The physical and chemical properties of eumelanin, Pigment Cell Res. 19 (2006) 572–594.
[36] P. Meredith, J. Riesz, Radiative relaxation quantum yields for synthetic eumelanin, Photochem. Photobiol. 79 (2007) 211–216.
[37] T. Saito, Y. Nishiyama, J. Putaux, M. Vignon, A. Isogai, Homogeneous suspensions of individualized microfibrils from TEMPO-catalyzed oxidation of native cellulose, Biomacromolecules 7 (2006) 1688–1691.
[38] L. Zhu, L. Zong, X. Wu, M. Li, H. Wang, J. You, C. Li, Shapeable fibrous aerogels of metal-organic-frameworks templated with nanocellulose for rapid and large-capacity adsorption, ACS Nano 12 (2018) 4462–4468.
[39] J. You, M. Li, B. Ding, X. Wu, C. Li, Crab chitin-based 2D soft nanomaterials for fully biobased electric devices, Adv. Mater. 29 (2017), 1606895.
[40] M. Li, L. Zong, W. Yang, X. Li, J. You, X. Wu, Z. Li, C. Li, Biological nanofibrous generator for electricity harvest from moist air flow, Adv. Funct. Mater. 29 (2019), 1901798.
[41] W. Yang, X. Li, X. Han, W. Zhang, Z. Wang, X. Ma, M. Li, C. Li, Asymmetric ionic aerogel of biologic nanofibrils for harvesting electricity from moisture, Nano Energy 71 (2020), 104610.
[42] W. Yang, L. Lv, X. Li, X. Han, M. Li, C. Li, Quaternized silk nanofibrils for electricity generation from moisture and ion rectification, ACS Nano 14 (2020) 10600–10607.
[43] Z. Li, J. Zhang, S. Zang, C. Yang, Y. Liu, F. Jing, H. Jing, J. Hu, C. Wang, Y. Zhou, Engineering controllable water transport of biosafety cuttlefish juice solar absorber toward remarkably enhanced solar-driven gas-liquid interfacial evaporation, Nano Energy 73 (2020), 104834.
[44] K. Wang, Y. Hou, B. Poudel, D. Yang, Y. Jiang, M. Kang, K. Wang, C. Wu, S. Priya, Melanin–perovskite composites for photothermal conversion, Adv. Energy Mater. 9 (2019), 1901753.
[45] D. Wu, Z. Wei, T. Mohamed, G. Zheng, F. Qu, F. Wang, Y. Zhao, C. Song, Lignocellulose biomass bioconversion during composting: mechanism of action of lignocellulase, pretreatment methods and future perspectives, Chemosphere 286 (2022), 131635.
[46] L. Zhang, X. Chen, Nanofluidics for giant power harvesting, Angew. Chem. Int. Ed. 52 (2013) 7640–7641.
[47] R. Zhang, S. Wang, M. Yeh, C. Pan, L. Lin, R. Yu, Y. Zhang, L. Zheng, Z. Jiao, Z. Wang, A streaming potential/current-based microfluidic direct current generator for self-powered nanosystems, Adv. Mater. 27 (2015) 6482–6487.
[48] N. Xu, X. Hu, W. Xu, X. Li, L. Zhou, S. Zhu, J. Zhu, Mushrooms as efficient solar steam-generation devices, Adv. Mater. 29 (2017), 1606762.
[49] X. Fan, Y. Yang, X. Shi, Y. Liu, H. Li, J. Liang, Y. Chen, A MXene-based hierarchical design enabling highly efficient and stable solar-water desalination with good salt resistance, Adv. Funct. Mater. 30 (2020), 2007110.

[50] P. Yang, K. Liu, Q. Chen, J. Li, J. Duan, G. Xue, Z. Xu, W. Xie, J. Zhou, Solar-driven simultaneous steam production and electricity generation from salinity, Energy Environ. Sci. 10 (2017) 1923–1927.
[51] B. Bourlon, J. Wong, C. Mikó, L. Forró, M. Bockrath, A nanoscale probe for fluidic and ionic transport, Nat. Nanotechnol. 2 (2007) 104–107.
[52] T. Ding, K. Liu, J. Li, G. Xue, Q. Chen, L. Huang, B. Hu, J. Zhou, All-printed porous carbon film for electricity generation from evaporation-driven water flow, Adv. Funct. Mater. 27 (2017), 1700551.
[53] D. Papanastasiou, A. Schultheiss, D. Muñoz-Rojas, C. Celle, A. Carella, J. Simonato, D. Bellet, Transparent heaters: a review, Adv. Funct. Mater. 30 (2020), 1910225.
[54] T. Sannicolo, M. Lagrange, A. Cabos, C. Celle, J. Simonato, D. Bellet, Metallic nanowire-based transparent electrodes for next generation flexible devices: a review, Small 12 (2016) 6052–6075.

Weiqing Yang received his M.S. degree from Qingdao University. Currently, He is a Ph.D. student in the Ningbo Institute of Materials Technology and Engineering, Chinese Academy of Sciences, under the supervision Professor Tao Chen and Peng Xiao. His current research interests focus on biomass/carbon-based composite construction and their applications as photo-thermal water purification and thermal management.

Dr. Peng Xiao received his Ph.D. in polymer chemistry and physics from Ningbo Institute of Materials Technology and Engineering, Chinese Academy of Sciences in 2017, under the supervision of Prof. Tao Chen. After that he joint Tao Chen's group as a postdoctoral research fellow. His current research interest focuses on the macroscopic self-assembly of 1D and 2D of carbon-based nanomaterials into 2D ultrathin films at air/water interface and further interfacial asymmetric modification to explore their potential applications in actuators, sensors and solar-to-thermal conversion.

Feng Ni received his B.S. degree from Tianjin Polytechnic University in 2017. Currently, he is a Ph.D. student in the Ningbo Institute of Materials Technology and Engineering, Chinese Academy of Sciences, under the supervision Professor Tao Chen. His current research interests focus on polymer/carbon based 2D hybrid materials and photo-thermal conversion.

Chang Zhang received his B.S. degree from Ningbo Institute of Technology, Zhejiang University, China in 2016. Currently, he is a master candidate in the Ningbo University and the Ningbo Institute of Materials Technology and Engineering, Chinese Academy of Sciences, under the supervision of Prof. Wenqin Wang and Prof. Tao Chen. His research interests focus on the carbon-based hybrid materials toward application of photo-thermal conversion.

Jincui Gu received her M.S. degree in material science from Hainan University. In 2012, she joint Tao Chen's group as an assistant researcher. Her current research focuses on construction of the polymer functionalized carbon-based membranes for water purification.

Prof. Shiao-Wei Kuo received his B.Sc. in chemical engineering from the National Chung Hsing University (1998) and Ph. D. in applied chemistry from the National Chiao Tung University in Taiwan (2002). He continued his research work at Chiao Tung University as a postdoctoral researcher during 2002–2007. Now, he is the professor in the Department of Materials and Optoelectronic Science, National Sun Yat-Sen University, Taiwan. His research interests include polymer interactions, self-assembly nanostructures, covalent organic frameworks, porous materials, POSS nanocomposites, polybenzoxazine, and polypeptides

Prof. Qingquan Liu received his Ph.D. in polymer chemistry and physics from Zhejiang University in 2009. Since 2009, he is a professor at Hunan University of Science and Technology. He joined National University of Singapore as an academic visitor during 2014–2015. His research interests include the preparation and application of microporous organic polymer materials, and preparation of water-based wax emulsions.

Prof. Tao Chen received his Ph.D. in polymer chemistry and physics from Zhejiang University in 2006. After his post-doctoral training at the University of Warwick (UK), he joined Duke University (USA) as a research scientist. He then moved back to Europe as an Alexander von Humboldt Research Fellow at Technische Universität Dresden, Germany. Since 2012, he is a full-time professor at Ningbo Institute of Materials Technology and Engineering, Chinese Academy of Sciences. His research interests include smart polymers and their hybrid systems with applications as actuators, shape memory polymers, and chemical sensing.